

Identification of a Bifunctional UDP-4-keto-pentose/UDP-xylose Synthase in the Plant Pathogenic Bacterium *Ralstonia solanacearum* Strain GMI1000, a Distinct Member of the 4,6-Dehydratase and Decarboxylase Family^{*[5]}

Received for publication, September 16, 2009, and in revised form, January 15, 2010. Published, JBC Papers in Press, January 29, 2010, DOI 10.1074/jbc.M109.066803

Xiaogang Gu[†], John Glushka[‡], Yanbin Yin[§], Ying Xu[§], Timothy Denny[¶], James Smith[‡], Yingnan Jiang[‡], and Maor Bar-Peled^{†||1}

From the [†]Complex Carbohydrate Research Center, the [§]Computational System Biology Laboratory, Department of Biochemistry and Molecular Biology, and the Institute of Bioinformatics, and the Departments of [¶]Plant Pathogen and ^{||}Plant Biology, University of Georgia, Athens, Georgia 30602

The UDP-sugar interconverting enzymes involved in UDP-GlcA metabolism are well described in eukaryotes but less is known in prokaryotes. Here we identify and characterize a gene (*RsU4kpxs*) from *Ralstonia solanacearum* str. GMI1000, which encodes a dual function enzyme not previously described. One activity is to decarboxylate UDP-glucuronic acid to UDP- β -L-threo-pentopyranosyl-4'-ulose in the presence of NAD⁺. The second activity converts UDP- β -L-threo-pentopyranosyl-4'-ulose and NADH to UDP-xylose and NAD⁺, albeit at a lower rate. Our data also suggest that following decarboxylation, there is stereospecific protonation at the C5 pro-R position. The identification of the *R. solanacearum* enzyme enables us to propose that the ancestral enzyme of UDP-xylose synthase and UDP-apiiose/UDP-xylose synthase was diverged to two distinct enzymatic activities in early bacteria. This separation gave rise to the current UDP-xylose synthase in animal, fungus, and plant as well as to the plant Uxs and bacterial ArnA and U4kpxs homologs.

UDP-xylose is an essential metabolite required to initiate synthesis of proteoglycans in humans and animals (1–3), synthesis of the acidic polysaccharide glucuronoxylomannan in the pathogenic fungus *Cryptococcus neoformans* (4–6), and synthesis of diverse plant polysaccharides such as xylan, xyloglucan, and xylogalacturonan (7, 8). Interestingly, xylosyl residues are rarely found in the bacteria or archaea analyzed to date. However, trace amounts of xylose were reported to be present in the lipopolysaccharide (LPS)² of certain strains of the human pathogens *Proteus mirabilis* (9) and *Ralstonia aeruginosa* (for-

merly *Pseudomonas aeruginosa*) (10, 11); in the gum-like polysaccharides secreted by *Aeromonas nichidenii* (12); and recently in the O-antigenic polysaccharide of the Gram-negative plant endosymbiont *Rhizobium leguminosarum* (13). How genes encoding enzymes forming UDP-xylose were evolved and why xylosyl residue appears predominantly in eukaryotes but scarce in bacteria remains unclear.

The metabolism of UDP-glucuronic acid (UDP-GlcA) varies among species (Fig. 1A). In animals, UDP-GlcA is reported to be converted only to UDP-xylose by UDP-GlcA decarboxylase (also named UDP-xylose synthase (Uxs)) (14), whereas plants can interconvert UDP-GlcA to UDP-apiiose by UDP-apiiose synthase (also named UDP-apiiose/UDP-xylose synthase (Uaxs)) (15, 16); to UDP-galacturonic acid (UDP-GalA) by UDP-GlcA 4-epimerase (17); and also to UDP-xylose by plant Uxs (18). Uaxs also produces UDP-xylose *in vitro*, albeit at a lower ratio compared with UDP-apiiose (16). In addition, one bacterium was reported to convert UDP-GlcA to UDP-L-Ara4O by the action of C-terminal ArnA as an intermediate for the synthesis of UDP- β -4-deoxy-4-formamido-L-arabinose (19).

We are interested in studying the metabolism of UDP-GlcA across all species with an aim to understand the origin and role of glycan diversity in biology. Such information may explain how the addition of new glycosyl residues to the specific polysaccharides provides new functions. Here, we report the first identification of a gene in the plant pathogen Gram-negative bacterium *Ralstonia solanacearum* str. GMI1000, which encodes an enzyme capable of converting UDP-GlcA to UDP-4-keto-pentose and subsequently at lower rate to UDP-xylose (Fig. 1B). The identification of this enzyme provides new insights related to UDP-GlcA metabolism and may help to explain how early plants or other eukaryotes obtained Uxs or Uaxs genes.

EXPERIMENTAL PROCEDURES

Phylogeny Analysis of Plant Uxs and Uaxs Homologs—The BLAST program (20) was used to identify proteins in the NCBI nonredundant data base that share high sequence similarity to functional plant Uaxs. Similarly, protein sequences of known Uxs were used to identify homologous proteins with an *E* value range between 1e-110 and 3e-25. The Uxs-like and Uaxs-like protein sequence data sets were merged. The CD-HIT program was used to select proteins where any two would have sequence

* This work was supported by National Science Foundation Grant IOB-0453664 (to M. B.-P.) and in part by the BioEnergy Science Center, which is supported by the Office of Biological and Environmental Research in the Department of Energy Office of Science.

[5] The on-line version of this article (available at <http://www.jbc.org>) contains supplemental Tables S1 and S2 and Figs. S1–S4.

¹ To whom correspondence should be addressed: CCRC 315 Riverbend Rd., Athens, GA 30602. Fax: 706-542-4412; E-mail: peled@ccrc.uga.edu.

² The abbreviations used are: LPS, lipopolysaccharide; UDP-4-keto-pentose, UDP- β -L-threo-pentopyranosyl-4'-ulose; RsU4kpxs, *R. solanacearum* UDP-4-keto-pentose/UDP-xylose synthase; UDP-GlcA, UDP-glucuronic acid; Uxs, UDP-xylose synthase; Uaxs, UDP-apiiose/UDP-xylose synthase; HPLC, high pressure liquid chromatography; MES, 4-morpholineethanesulfonic acid; L-Ara4N, 4-amino-4-deoxy-L-arabinose.

UDP-4-keto-pentose/UDP-xylose Synthase in *R. solanacearum*

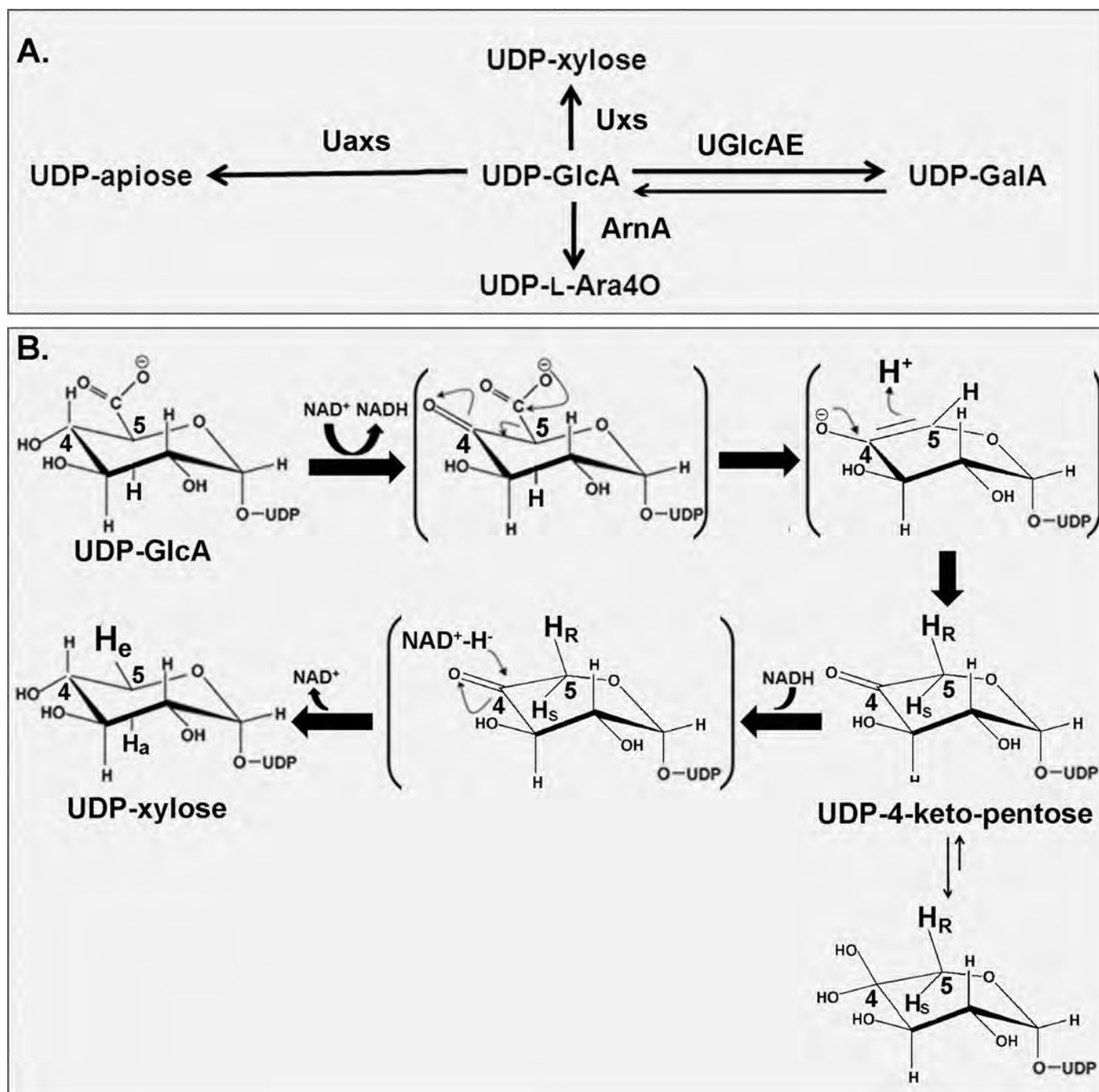


FIGURE 1. **UDP-GlcA metabolism in eukaryote and prokaryote.** *A*, in animals, some fungi and plants, UDP-GlcA is converted to UDP-xylose by UDP-GlcA decarboxylase (also named Uxs). Plants and several bacteria (such as *Streptococcus pneumoniae*) consist of UDP-GlcA 4-epimerase (UGlcAE) that interconverts UDP-GlcA and UDP-GaIA. Plants also have a bifunctional UDP-apiose synthase/Uaxs that can interconvert UDP-GlcA to UDP-apiose and UDP-xylose. In some bacteria, UDP-GlcA can be converted into UDP-L-Ara4O in the presence of ArnA. *B*, the proposed enzymatic activities of UDP-4-keto-pentose synthase and subsequent UDP-xylose synthase. In the presence of NAD⁺, UDP-GlcA is decarboxylated to UDP-4-keto-pentose and NADH. The final protonation at C5 is stereoselective (*H_R* in **bold type**). In solution, UDP-4-keto-pentose exists predominantly as the gem-diol hydrate form (see *bottom right*). The U4kpxs enzyme is bifunctional, and the released UDP-4-keto-pentose in the presence of NADH can be converted to UDP-xylose and NAD⁺, albeit at a lower rate when compared with the first activity. *H_R* and *H_S* indicate the pro-R H5 and pro-S H5 of UDP-4-keto-pentose, whereas *H_a* and *H_e* indicate the axial H5 and equatorial H5 of UDP-xylose, respectively.

identity lower than 95%. The processed sequence data were reduced to a final set of total 135 proteins. The conserved Pfam epimerase domains in the final set proteins were used for the multiple sequence alignment and for the subsequent phylogenetic analysis. The multiple sequence alignment was built using the MAFFT v6.603 program (21), and the resulting alignment

was used to perform maximum likelihood phylogeny reconstruction using the PhyML v2.4.4 program (22). Several protein candidates were selected for further work.

cDNA Cloning—Genomic DNA was isolated from *R. solanacearum* str. GMI1000. The coding sequence (NP_519440.1) of the putative *Ralstonia* protein that has an E

UDP-4-keto-pentose/UDP-xylose Synthase in *R. solanacearum*

value of $4e-62$ to the potato Uaxs (StUaxs) (16) and an E value of $9e-32$ to *Arabidopsis* Uxs3 (AtUxs3) (18) was amplified by PCR using 1 unit of high fidelity proofreading Platinum DNA polymerase (Invitrogen) and $0.2 \mu\text{M}$ of each forward and reverse primers: 5'-TCATGAAGAAAGTACTGATCCTCGGCGTC-3' and 5'-AAGCTTGTCGACCAGGCTGCGCGCC-3'. The PCR product was cloned to generate plasmid pGEM-T:RsGM#4 and verified by sequencing (GenBankTM accession number GQ369438). The BspHI-HindIII fragment (1061bp) containing the full-length gene (from now on named UDP-4-keto-pentose/UDP-xylose synthase (*RsU4kpxs*)) without the stop codon was subcloned into an *Escherichia coli* expression vector derived from pET28b (23) to generate pET28b:RsU4kpxs#1 that will add six histidines to the C terminus of the recombinant RsU4kpxs.

Protein Expression and Purification—*E. coli* cells containing pET28b:RsU4kpxs#1 or an empty vector (control) were cultured for 16 h at 37°C in LB medium (20 ml) supplemented with kanamycin ($50 \mu\text{g}/\text{ml}$) and chloramphenicol ($34 \mu\text{g}/\text{ml}$). A portion (7 ml) of the cultured cells was transferred into fresh LB liquid medium (250 ml) supplemented with the same antibiotics, and the cells were then grown at 37°C at 250 rpm until the cell density reached $A_{600} = 0.6$. The cultures were then transferred to 30°C , and gene expression was induced by the addition of isopropyl β -D-thiogalactoside to a final concentration of 0.5 mM . After 4 h of growth while shaking (250 rpm), the cells were harvested by centrifugation ($6,000 \times g$ for 10 min at 4°C), resuspended in lysis buffer (10 ml 50 mM sodium phosphate, pH 7.5, containing 10% (v/v) glycerol, 1 mM EDTA, 1 mM dithiothreitol, and 0.5 mM phenylmethylsulfonyl fluoride), and lysed in an ice bath by 24 sonication cycles (10-s pulse; 20-s rest) using a Misonix S-4000 (Misonix Inc., Farmingdale, NY) equipped with microtip probe. The lysed cells were centrifuged at 4°C for 10 min at $6,000 \times g$, and the supernatant was supplemented with 1 mM dithiothreitol and centrifuged again (30 min at $20,000 \times g$). The resulting supernatant (termed s20) was recovered and kept at -20°C .

His-tagged protein was purified on a column (10-mm inner diameter \times 150 mm long) containing 2 ml of nickel-Sepharose (Qiagen) equilibrated with 50 mM sodium phosphate, pH 7.5, containing 0.3 M NaCl. The bound His-tagged protein was eluted with the same buffer containing increasing concentrations of imidazole. The fractions containing RsU4kpxs activity were pooled, supplemented with 1 mM dithiothreitol, flash frozen in liquid nitrogen, and stored in aliquots at -80°C . Proteins extracted from *E. coli* cells expressing empty vector were passed via the same nickel column, and fractions eluted with imidazole were collected and served as controls in enzyme assays and SDS-PAGE analyses. The concentration of proteins was determined using the Bradford reagent using bovine serum albumin as standard.

The molecular masses of the recombinant proteins were estimated by size exclusion chromatography using a Waters 626 LC HPLC system equipped with a photodiode array detector (PDA 996) and a Waters Millennium32 work station. Separate solutions (0.5 ml) of RsU4kpxs or a mixture of standard proteins (2 mg each of aldolase (157 kDa), bovine serum albumin (68 kDa), carbonic anhydrase (29 kDa), and cytochrome *c* (12.4 kDa)) were separately chromatographed at 0.5 ml min^{-1} on a Superdex75 column (10-mm inner diameter \times 300 mm long;

GE Healthcare) equilibrated with 20 mM Tris-HCl, pH 7.6, containing 0.1 M NaCl. The eluant was monitored at 280 nm, and the fractions were collected every 30 s. The fractions containing enzyme activity were pooled and kept at -80°C .

HPLC-based Enzyme Assay—Unless otherwise indicated, RsU4kpxs reactions (final volume, $50 \mu\text{l}$) consisted of 50 mM sodium phosphate, pH 7.6, 1 mM NAD^+ , 1 mM UDP-GlcA, and $1 \mu\text{g}$ of recombinant RsU4kpxs. The reactions were kept at 37°C for up to 20 min and then terminated by boiling (100°C , 2 min). An equal volume of chloroform was added, and after vortexing (30 s) and centrifugation (12,000 rpm for 5 min, at room temperature), the upper aqueous phase was collected and chromatographed (17) on a Q15 anion exchange column (2-mm inner diameter \times 250 mm long; Amersham Biosciences) using an Agilent Series 1100 HPLC system equipped with an autosampler, diode array detector and ChemStation software. Alternatively, reaction products were separated on a Prep C18 Scalar column (4.6-mm inner diameter \times 250 mm long; Agilent) using 20 mM *tert*-butylamine- H_3PO_4 , pH 6.6, in 20% methanol. The nucleotides were detected by their UV absorbance using the Agilent photodiode array detector. The maximum absorbance for UDP-sugars, NAD^+ , and NADH were 261, 259, and 259/340 nm, respectively, in ammonium formate and *tert*-butylamine- H_3PO_4 , pH 6.6, in 20% methanol. The peak areas of analytes were compared with calibration curves of internal standards (UDP-Glc, UDP-GlcA, and NADH) and used to calculate the amount of products formed. The enzyme reaction was also done in a D_2O solution as described above, except that the buffer was made in 99% D_2O , to which the enzyme was added, giving a final solution containing 90% D_2O .

Real Time ^1H NMR-based Assay—Two types of real time NMR assays were performed at 37°C each in a total volume of $180 \mu\text{l}$. The D_2O reactions were performed in a final mixture of $\text{D}_2\text{O}:\text{H}_2\text{O}$ (9:1 v/v) and contained 50 mM sodium phosphate, pH, pD 7.6, 1 mM UDP-GlcA, 1 mM NAD^+ , and $3 \mu\text{g}$ of recombinant RsU4kpxs. The purified enzyme was supplied in H_2O buffer. The H_2O reactions were identical but performed in a final solution of 10% D_2O and 90% H_2O . After the addition of the enzyme, the reaction mixture was transferred to a 3-mm NMR tube. Real time ^1H NMR spectra were obtained using a Varian DirectDriveTM 600-MHz spectrometer equipped with a cryogenic probe. Data acquisition was started ~ 5 min after the addition of enzyme to optimize the spectrometer. Sequential one-dimensional proton spectra with presaturation of the water resonance were acquired over the course of the enzymatic reaction. Spectra of individual 1 mM standards of NAD^+ , UDP-xylose, UDP-GlcA, and NADH prepared in the same buffer were collected with the same temperature and parameter settings. Additional NMR analyses were performed using Varian DirectDriveTM 900-MHz spectrometer. All of the spectra at 37°C were referenced to the water resonance at 4.63 ppm downfield of 2,2-dimethyl-2-silapentane-5-sulfonate; the spectra at 25°C were referenced to water at 4.76 ppm.

Enzyme Properties of RsU4kpxs—The enzyme activity was tested in a variety of buffers, at different temperatures, different ions, or with different potential inhibitors. For optimal pH

UDP-4-keto-pentose/UDP-xylose Synthase in *R. solanacearum*

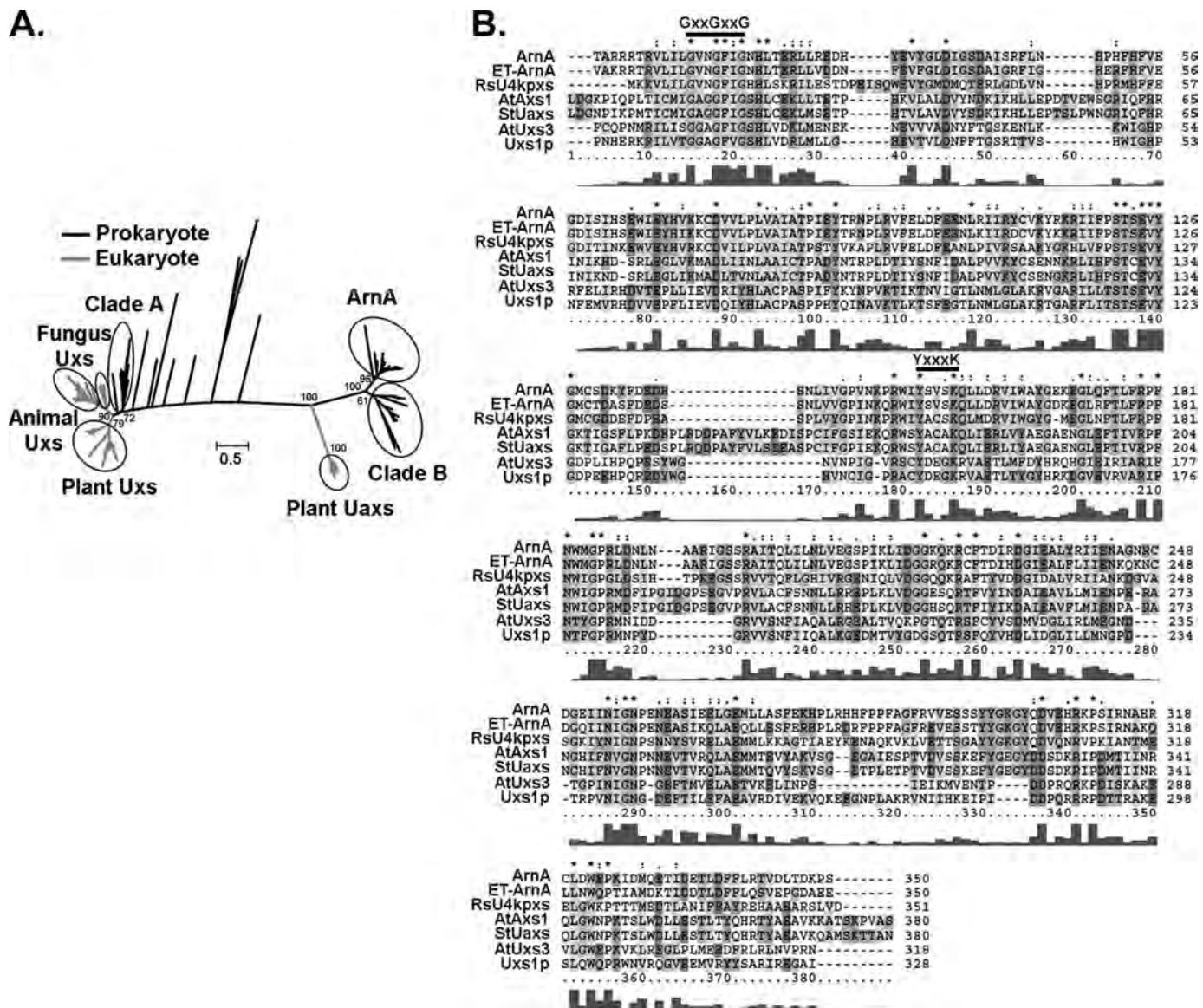


FIGURE 2. Protein sequence alignments and phylogenetic relationship of Uxs-like and Uaxs-like proteins from diverse species. A, phylogenetic relationships of selected Uxs-like and Uaxs-like proteins. Protein sequences were aligned and analyzed using the MAFFT program, and the phylogenetic trees were created using the PhyML program. The bootstrap values for the clades are shown. The bar represents 0.5-amino acid substitutions per site. B, protein sequences of *Arabidopsis* AtUxs3 (NP_001078768, amino acids 40–375), of *C. neoformans* Uxs1p (AAM22494, amino acids 83–410), of potato StUxs (ABC75032, amino acids 7–386), of *Arabidopsis* AtAxs1 (AAC73015, amino acids 10–389), of Arna (AY057445, amino acids 311–660), of *Erwinia tasmaniensis* Arna homolog, Et-Arna (YP_001908305, amino acids 311–660), and of full-length RsU4kpxs (GQ369438) were aligned with ClustalX software, and the conserved motifs are shown.

experiments, 1 μ g of recombinant enzyme was first mixed with 1 mM UDP-GlcA and 50 mM of each individual buffer (Tris-HCl, sodium phosphate, MES, or HEPES). NAD⁺ (1 mM) was then added, and after 20 min of incubation at 37 °C, the amount of UDP-4-keto-pentose formed was determined by HPLC. Inhibition assays were performed by first mixing the enzyme and sodium phosphate buffer with various additives (e.g. nucleotides) on ice for 10 min. UDP-GlcA and NAD⁺ (1 mM each) were then added. After 20 min at 37 °C, the amount of UDP-4-keto-pentose formed was calculated from the HPLC chromatogram. For the optimal temperature experiments, the assays were performed under standard conditions except that reactions were incubated at different temperature for 20 min. Subsequently, the activities were terminated (100 °C),

and the amount of UDP-4-keto-pentose was measured by HPLC.

RESULTS

Identification, Cloning, and Characterization of Ralstonia UDP- β -L-threo-pentopyranosyl-4''-ulose Synthase, RsU4kpxs—As described in the introduction, several enzymes are known to interconvert UDP-GlcA to other UDP-sugars. These proteins contain two conserved motifs that are also common in other NDP-sugar interconverting enzymes such as 4,6-dehydratases, and 4-epimerases (24). At the N-terminal region of these proteins is the GXXGXXG domain that binds the cofactor NAD⁺ (25), and ~100 amino acids downstream is the YXXXX motif (26) that is involved in catalysis. Aside from these conserved

UDP-4-keto-pentose/UDP-xylose Synthase in *R. solanacearum*

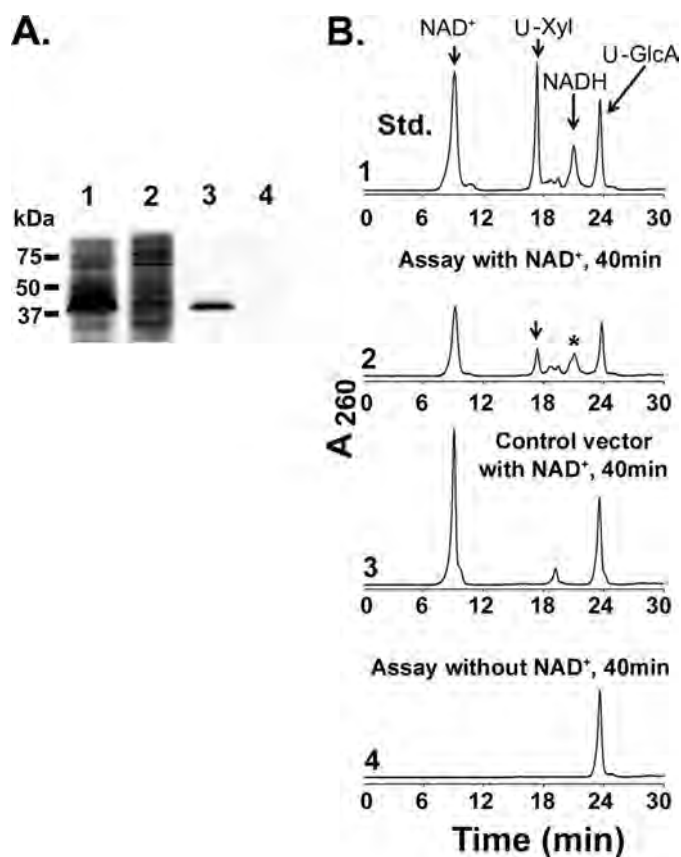


FIGURE 3. Expression and initial characterization of recombinant RsU4kpxs. *A*, SDS-PAGE of total soluble protein isolated from *E. coli* cells expressing RsU4kpxs (lane 1) or control empty vector (lane 2), and after purification over nickel column (lane 3, RsU4kpxs; lane 4, control). *B*, HPLC chromatogram of RsU4kpxs enzyme reaction. Purified recombinant RsU4kpxs was incubated with UDP-GlcA for 40 min in the presence (panel 2) or absence (panel 4) of exogenous NAD⁺. As a control, the corresponding column-purified protein isolated from cells expressing control empty vector was incubated with UDP-GlcA and NAD⁺ for 40 min (panel 3). The reaction products were separated with a Q15 column. The distinct UDP-sugar peak (marked by arrow, in panel 2) was collected and analyzed by NMR, and the NADH peak in panel 2 is marked by an asterisk.

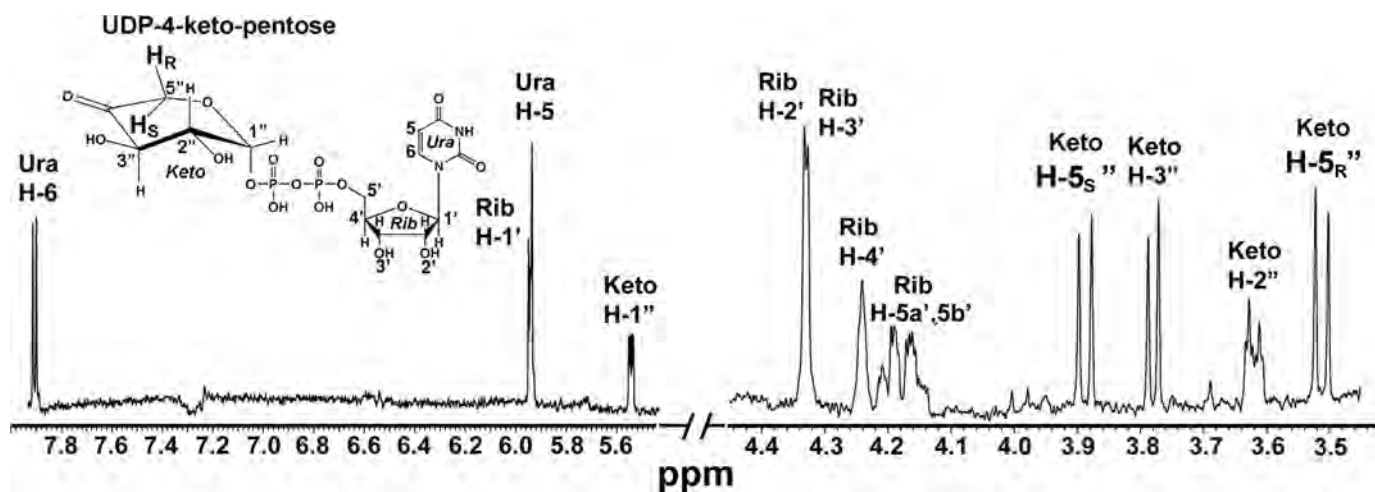


FIGURE 4. ¹H NMR analysis of the RsU4kpxs product, UDP-β-L-threo-pentopyranosyl-4'-ulose (UDP-4-keto-pentose). The enzymatic product (Fig. 3B, panel 2, marked by arrow) was collected and analyzed by NMR at 37 °C. One-dimensional 600-MHz NMR spectrum of the product is shown in selected regions between 3.5 and 4.4 and between 5.5 and 8.0 ppm. The location for each proton residue on the spectrum is indicated: the position of protons on the uracil (Ura) ring are indicated by *H*, the ribose (Rib) protons are indicated by *H'*, and the 4-keto-pentose protons are indicated by *H''*. Note the diagnostic doublet signal for each of C5 protons: pro-R H5 (3.51 ppm) and pro-S H5 (3.89 ppm).

motifs, the above enzymes do have amino acid differences that account for their substrate specificity and catalytic properties.

The maximum likelihood phylogenetic tree shown in Fig. 2A indicates that there are five major clades for proteins related to Uxs and Uaxs: a eukaryote Uxs clade, a plant Uaxs clade, an ArnA (19) clade, and two additional clades (A and B) with unknown functions. Members belonging to clades A, B, and ArnA are mostly bacteria (Fig. 2A). A clade B protein from *R. solanacearum* str. GMI1000 was chosen as a possible link to the ancestral origin of enzymes that produce UDP-apiose and UDP-xylose. There are other bacterial proteins in clade B. Some belong to human pathogenic species such as *Burkholderia cenocepacia*, but others are nonpathogenic species including *Geobacter bemidjiensis*. The *R. solanacearum* protein that we selected shares 28% amino acid identity to *Arabidopsis* AtUxs3, 35% identity to potato StUaxs, and higher identity (53%) to the bacterial ArnA C-terminal domain from *E. coli* (Fig. 2B). The *Ralstonia* protein differs from ArnA having a short six-amino acid extension peptide after the GXXGXXG motif and appears to share no sequence similarity in amino acids 270–290 and 330–350 (supplemental Fig. S1). To determine whether these amino acid differences alter the specific activity of the *Ralstonia* enzyme, the encoded gene was expressed in *E. coli*, purified, and subsequently characterized.

Compared with control, a highly expressed protein band (41 kDa) was detected after SDS-PAGE analysis of *E. coli* cells expressing recombinant *R. solanacearum* protein (Fig. 3A, lane 1). The protein was column-purified (Fig. 3A, lane 3), and preliminary HPLC-based experiments demonstrated that both the crude and purified protein converts UDP-GlcA and NAD⁺ to a UDP-sugar and NADH. NADH was confirmed as an enzymatic product based on its specific dual UV absorbance at 259 and 340 nm, and its HPLC chromatograph was identical as authentic NADH standard (Fig. 3B, panel 2). To determine the identity of the other product, the reaction with purified enzyme was separated by Q15 anion exchange column, and the product peak eluted at 17.2 min (Fig. 3B, panel 2, marked by arrow) was

UDP-4-keto-pentose/UDP-xylose Synthase in *R. solanacearum*

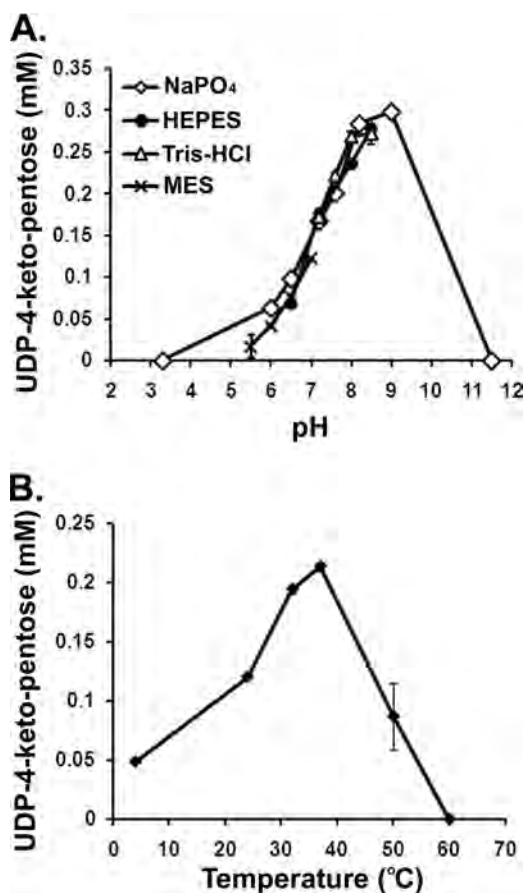


FIGURE 5. The effects of buffer composition, pH and temperature on UDP-4-keto-pentose synthase activity. *A*, the activity of recombinant RsU4kpxs was analyzed at different buffers (Tris-HCl, sodium phosphate, MES, or HEPES) at different pH. Each value is the mean of triplicate reactions. *B*, the activity of recombinant RsU4kpxs was analyzed at different temperatures in 50 mM sodium phosphate buffer, pH 7.6. Each value is the mean of triplicate reactions.

collected and analyzed by ^1H NMR. The NMR spectrum (Fig. 4 and supplemental Table S1) provided chemical shifts consistent with UDP- β -*L*-threo-pentopyranosyl-4''-ulose (herein referred to as UDP-4-keto-pentose), previously reported as the enzymatic product of ArnA (19). Consistent with the report by Breazeale *et al.* (19), no nuclear Overhauser effect was observed between the H5 protons and any other ring protons (data not shown), preventing the identification of pro-R and pro-S H5 by conventional methods. However, the NMR analysis of selectively deuterated enzymatic products discussed later in this paper provided the assignment of H5 protons that is reversed from the Breazeale *et al.* (19) report. Although the compound has been shown to exist primarily in the gem-diol hydrated form in aqueous solution (19), it is depicted in Fig. 4 as the keto-form for simplicity. Thus the function of the gene encoding RsU4kpxs protein is confirmed as a UDP-4-keto-pentose synthase.

Characterization and Properties of Recombinant UDP-4-keto-pentose Synthase—The purified recombinant enzyme is stable if it was flash frozen after purification. Like Uxs and Uaxs, RsU4kpxs does not require metals for activity and remains fully active in the presence of EDTA (supplemental Table S2). The enzyme is active between pH 5 and pH 9 (Fig. 5A) with maxi-

TABLE 1
Enzymatic kinetics of the bi-functional recombinant RsU4kpxs

	Synthase activity
UDP-4-keto-pentose^a	
K_m , UDP-GlcA (μM)	22.2 ± 1.2
K_m , NAD^+ (μM)	113.2 ± 4.1
V_{max} , UDP-GlcA ($\mu\text{M min}^{-1}$)	4.2 ± 0.3
V_{max} , NAD^+ ($\mu\text{M min}^{-1}$)	4.7 ± 0.3
k_{cat} , UDP-GlcA (min^{-1})	17.1 ± 1.2
k_{cat} , NAD^+ (min^{-1})	19.2 ± 1.4
k_{cat}/K_m (UDP-GlcA) ($\text{mM}^{-1} \text{s}^{-1}$)	12.8 ± 0.3
k_{cat}/K_m (NAD^+) ($\text{mM}^{-1} \text{s}^{-1}$)	2.8 ± 0.3
UDP-xylose^b	
K_m , UDP-4-keto-pentose (μM)	152.9 ± 22.3
K_m , NADH (μM)	94.2 ± 12.7
V_{max} , UDP-4-keto-pentose ($\mu\text{M min}^{-1}$)	3.6 ± 0.2
V_{max} , NADH ($\mu\text{M min}^{-1}$)	3.9 ± 0.1
k_{cat} , UDP-4-keto-pentose (min^{-1})	0.73 ± 0.05
k_{cat} , NADH (min^{-1})	0.81 ± 0.01
k_{cat}/K_m (UDP-4-keto-pentose) ($\text{mM}^{-1} \text{s}^{-1}$)	0.081 ± 0.009
k_{cat}/K_m (NADH) ($\text{mM}^{-1} \text{s}^{-1}$)	0.15 ± 0.01

^a UDP-4-keto-pentose synthase activity was measured with varied concentrations of UDP-GlcA (0.08–1.0 mM) or NAD^+ (0.08–1.0 mM) in the presence of 0.5 μg of enzyme after 10 min at standard conditions. The reciprocal initial velocity was plotted against the reciprocal UDP-GlcA or NAD^+ concentration according to Lineweaver and Burk to calculate the corresponding K_m values. The data presented are the average K_m values from three experiments.

^b UDP-xylose synthase activity was measured with varied concentrations of UDP-4-keto-pentose (0.075–0.3 mM) or NAD^+ (0.1–0.4 mM) in the presence of 10 μg of enzyme after 20 min of reaction. The reciprocal initial velocity was plotted against the reciprocal UDP-4-keto-pentose or NADH concentration according to Lineweaver and Burk to calculate the corresponding K_m values. The data presented are the average K_m values from three experiments.

mum activity at 37 °C (Fig. 5B). RsU4kpxs was inhibited by UDP and NADH but not by other nucleotides or nucleotide-sugars (supplemental Table S3). To investigate cofactor and nucleotide-sugar specificity, the enzyme was reacted for up to 60 min with the NAD^+ analog NADP^+ or with the UDP-GlcA isomer UDP-GalA, and in both cases activity was not observed (data not shown). Thus we concluded that the recombinant enzyme is specific for NAD^+ and UDP-GlcA. The molecular size of the active RsU4kpxs was determined by size exclusion chromatography. The active fraction migrated as a globular protein having a mass between 80 and 120 kDa, suggesting that RsU4kpxs is not a monomer, possibly a dimer. Kinetics analyses of the UDP-4-keto-pentose synthase activity of RsU4kpxs are summarized in Table 1. The apparent K_m values were 22.2 (UDP-GlcA) and 113.2 μM (NAD^+), V_{max} values ($\mu\text{M min}^{-1}$) were 4.2 for UDP-GlcA and 4.7 for NAD^+ , and the k_{cat}/K_m values ($\text{s}^{-1} \text{mM}^{-1}$) were 12.8 (UDP-GlcA) and 2.8 (NAD^+).

Real Time NMR Analysis of UDP-4-keto-pentose Synthase, RsU4kpxs— ^1H NMR spectroscopy is an important tool to monitor enzymatic reactions in real time (16, 17, 27, 28). This procedure is ideal for analyzing the time-dependent appearance and disappearance of intermediates and the detection of unstable products.

NMR-based RsU4kpxs enzyme reactions were first done in 90% D_2O to reduce the interference of the water signal. Over the time of the reaction, as shown in Fig. 6A, the peaks corresponding to NAD^+ (N) and UDP-GlcA (G) decreased, and simultaneously, peaks corresponding to NADH (H) and UDP-4-keto-pentose (K) increased. However, in addition to the expected proton doublet for K5s (3.89 ppm), an additional singlet peak (marked by an arrow in Fig. 6A, and see inset for an expansion view) was also observed to increase at the same rate. To identify the molecule that gives rise to the singlet peak, the

UDP-4-keto-pentose/UDP-xylose Synthase in *R. solanacearum*

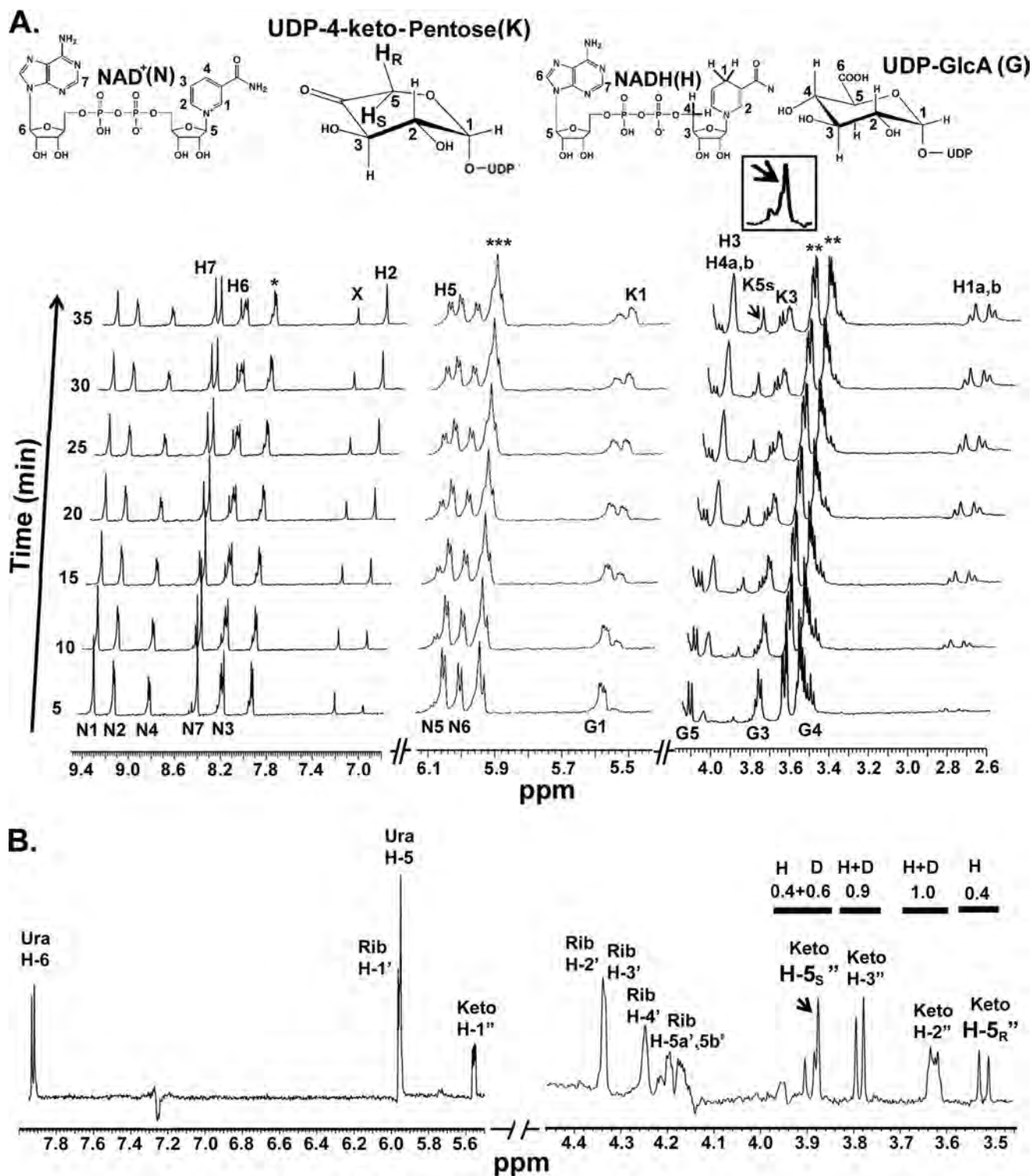


FIGURE 6. Real time ^1H NMR analyses of UDP-4-keto-pentose synthase activity performed in D_2O . *A*, purified recombinant RsU4kpxs was mixed with UDP-GlcA, buffer, and NAD^+ (in a final mixture of 9:1 $\text{D}_2\text{O}/\text{H}_2\text{O}$). Approximately 5 min after enzyme addition and NMR shimming, NMR data were collected (*bottom trace*). Selected regions (from 2.6 to 4.2, 5.5 to 6.1, and 7.0 to 9.4 ppm) of the spectra from 5 to 35 min are shown. The signals are labeled as indicated by the compounds above the spectrum: protons belonging to NAD^+ (N), NADH (H), UDP-4-keto-pentose (K), and UDP-GlcA (G). The single peak (indicated by an *arrow*) for UDP-4-keto-pentose pro-S H5 is due to the selective deuteration of its pro-R H5. The *inset* shows expansion of the pro-S H5 signal(s) that arose from a mixture of deuterated and fully protonated molecular species of UDP-4-keto-pentose. The enzyme activity during real time NMR was carried out at 37 °C. Peaks marked by * (from 7.9 to 8.0 ppm) are the mixture of signals for Ura-H6 proton of UDP-4-keto-pentose and UDP-GlcA. Peaks marked by ** (from 3.5 to 3.7 ppm) are the mixture of signals for the G2, K2, K5_R , and glycerol protons derived from the enzyme preparation. Peaks marked by *** (from 5.9 to 6.0 ppm) are the mixture of signals for Rib-H1' and Ura-H5 protons of UDP-4-keto-pentose and UDP-GlcA. X indicates an impurity resonance. *B*, recombinant RsU4kpxs was incubated with NAD^+ , UDP-GlcA, and buffer in a final mixture of 90% D_2O . The enzymatic product was separated by HPLC, and the UDP-4-keto-pentose peak was collected and analyzed by ^1H NMR. One-dimensional 600-MHz NMR spectrum (operated at 37 °C) of the UDP-4-keto-pentose is shown from 3.5 to 4.5 and 5.5 to 8.0 ppm. The signals are labeled as in Fig. 3, and the single peak for UDP-4-keto-pentose pro-S H5, where pro-R H5 is deuterated, is indicated by an *arrow*. Integration of peaks shows that 60% are in deuterated UDP-4-keto-pentose form (D) and 40% are protonated (H).

UDP-4-keto-pentose/UDP-xylose Synthase in *R. solanacearum*

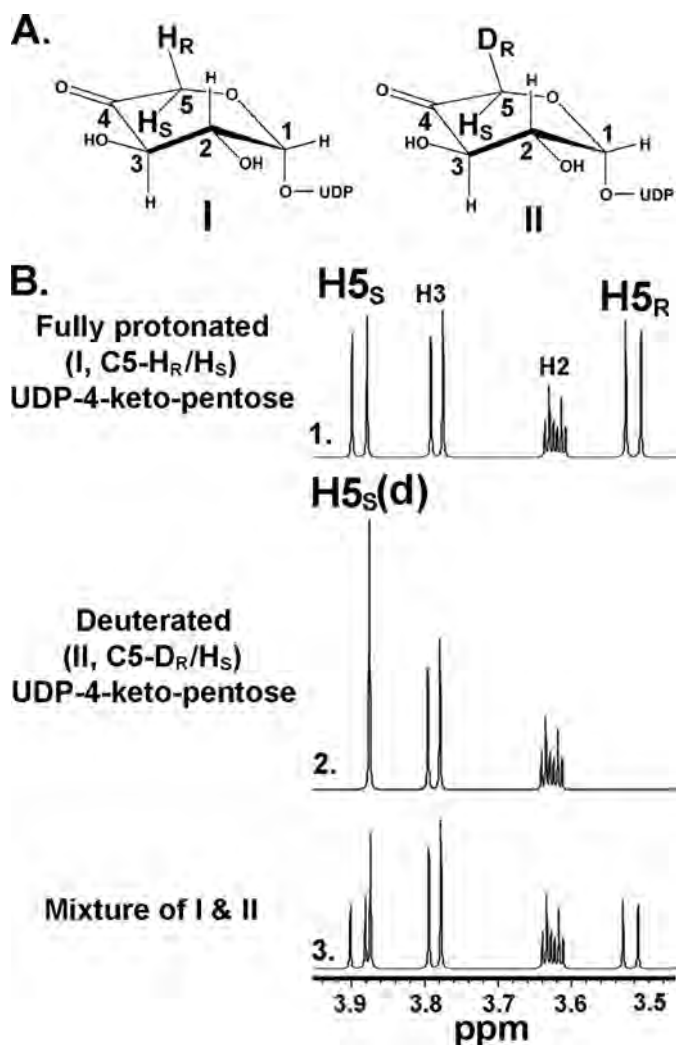


FIGURE 7. Illustration of NMR spectra for enzymatic derived UDP-4-keto-pentose species. A, UDP-4-keto-pentose is made as fully protonated (panel I, C5-H_R/H_S) and pro-R H5 deuterated (panel II, C5-D_R/H_S) forms. B, simulated NMR spectrum when both C5 H_S and H_R are protonated (panel 1), and when C5 pro-R proton is deuterated (D_R) (panel 2). Note the pro-S in panel 2 is protonated (H_S). Panel 3 shows the simulated spectrum of the mixture (panels I and II). The pro-R and pro-S protons at C5 are labeled as H_{5R} and H_{5S}, respectively. The pro-S proton where the pro-R position is deuterated is labeled as H_{5S(d)}. The simulations (Spinevolution program) (31) shown are the selected regions of the ¹H NMR spectra for protons belong to C5, C2, and C3.

HPLC-based enzyme assays were carried out in 90% D₂O rather than in H₂O, and the UDP-4-keto-pentose product was purified. Fig. 6B clearly shows that the product is comprised of two molecular species of UDP-4-keto-pentose: one fully protonated at C5 and the other deuterated at the C5-pro-R position (Fig. 7A). Description of this mixture of enzymatic-formed species is illustrated in Fig. 7B. Integration of the protons at C5 indicates that 60% of the UDP-4-keto-pentose is deuterated (Fig. 6B). Although the pro-S H5 peak is coupled to the geminal pro-R D5, the scalar coupling is less than 2 Hz and is not resolved, giving a singlet shifted by 11 Hz because of an isotope effect. Repeating the real time NMR assay in 90% H₂O produced the normal fully protonated product (Fig. 8) as expected.

The lack of any corresponding singlet in the pro-R H5 region (3.51ppm) suggests that the incorporation of the deuterated proton is stereospecific. This observation may support the

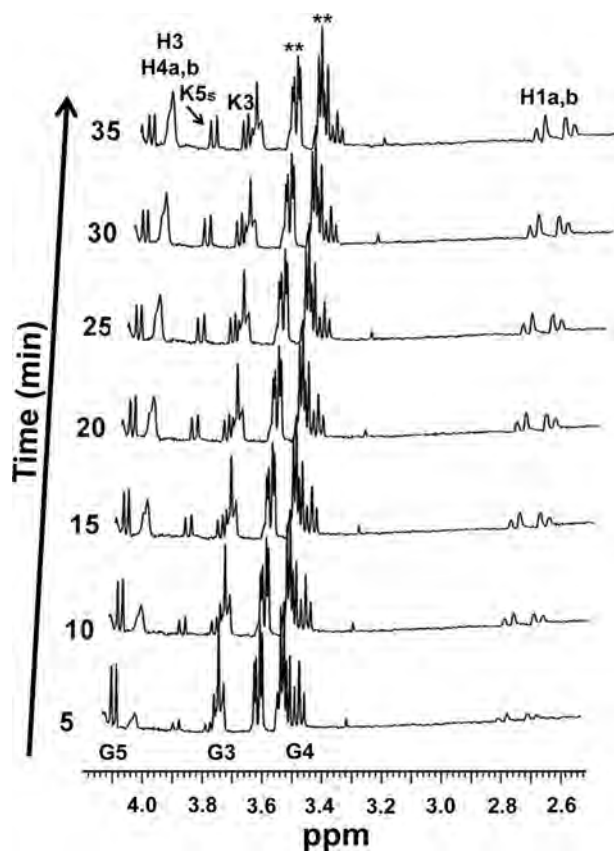


FIGURE 8. Real time ¹H NMR analyses of UDP-4-keto-pentose synthase activity performed in H₂O. Purified recombinant RsU4kpxs was mixed with UDP-GlcA, buffer, and NAD⁺ in a final mixture of H₂O/D₂O (9:1 v/v). Approximately 5 min after enzyme addition and NMR shimming, the NMR data were collected (bottom trace). The enzyme activity during real time NMR was carried out at 37 °C. Selected region of the ¹H NMR spectra from 2.6 to 4.2 ppm and from 5 to 35 min are shown. The signals are labeled as indicated by the compounds shown in Fig. 6A. The doublet peak of the pro-S H5 of UDP-4-keto-pentose is marked by an arrow. The peaks marked by ** (from 3.5 to 3.7ppm) are mixtures of signals for the G2, K2, K_{5R}, and glycerol protons derived from the enzyme preparation.

mechanism of Williams *et al.* (29) and Gatzeva-Topalova *et al.* (30), who proposed that following the abstraction of the C4 hydride and formation of the UDP-4-keto sugar, decarboxylation is mediated by an enzyme-assisted mechanism rather than a spontaneous event.

RsU4kpxs Can Also Convert UDP-4-keto-pentose with NADH to UDP-xylose—When the purified *Ralstonia* enzyme (1 μg) was incubated with UDP-GlcA and NAD⁺ for longer period of times, in addition to the major product of UDP-4-keto-pentose (Fig. 9A, panels 5 and 6, marked by the asterisk), it yielded small amount of a new product with the retention time (9.3 min) corresponding to standard UDP-xylose (Fig. 9A, panel 5 and 6, marked by arrow). The appearance of a peak at 5.47 ppm corresponding to H1 of UDP-xylose was also observed when NMR assays were carried out for a longer time (data not shown). When assays were performed with 10 μg of recombinant protein, the formation of UDP-xylose as well as UDP-4-keto-pentose was observed (Fig. 9B), suggesting that the enzyme may have dual functions.

To address whether the UDP-xylose product is directly converted from UDP-4-keto-pentose, the recombinant RsU4kpxs

UDP-4-keto-pentose/UDP-xylose Synthase in *R. solanacearum*

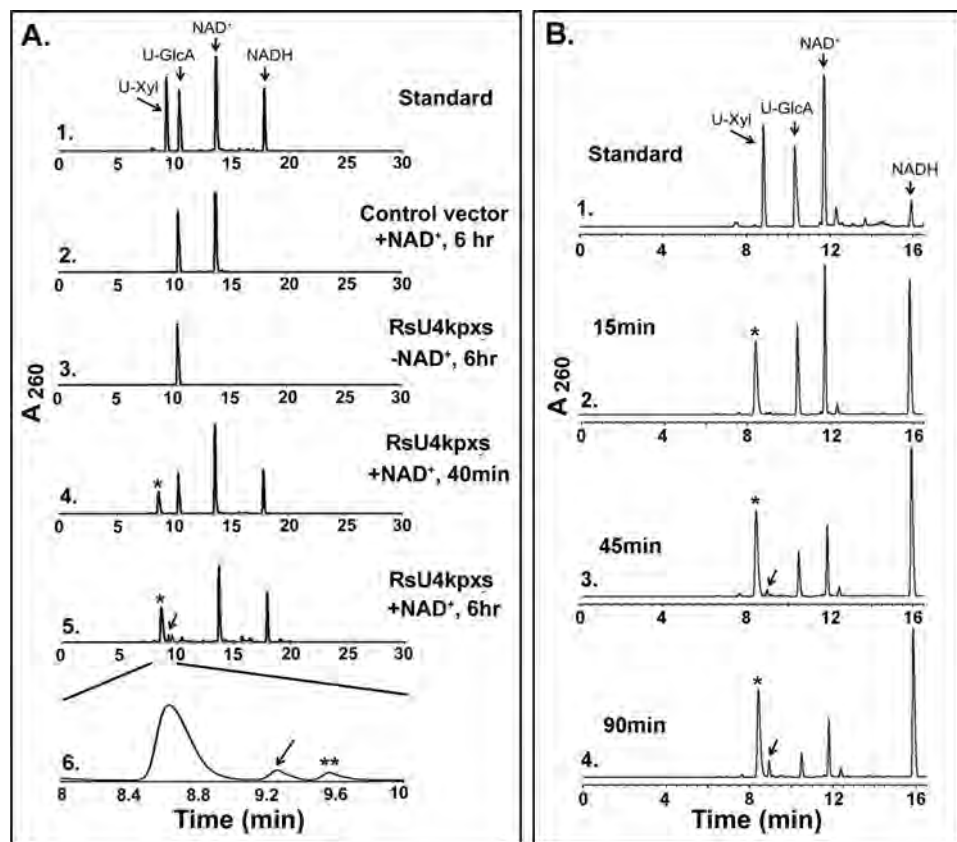


FIGURE 9. RsU4kpxs is a bifunctional enzyme and converts UDP-GlcA to UDP-4-keto-pentose and subsequently to UDP-xylose. *A*, purified recombinant RsU4kpxs (1 μ g) was mixed under normal assay conditions with UDP-GlcA, buffer, and NAD⁺ at 37 °C for 40 min (*panel 4*), or 6 h (*panel 5* and *6*). The reactions were also performed without NAD⁺ for 6 h (*panel 3*). As a control, the corresponding column-purified protein isolated from cells expressing empty vector was incubated with UDP-GlcA and NAD⁺ for 6 h (*panel 2*). The reaction products were separated on a C18 column (Agilent prep-C18 scalar), and chromatograms are shown. UDP-4-keto-pentose is marked by an asterisk (*panel 4* and *5*), and the new peak (eluted at 9.3 min, as UDP-xylose) is marked by an arrow (*panel 5* and *6*). *Panel 6* is an expanded view of *panel 5* between 8 and 10 min. The identity of the small peak eluted at 9.5 min (marked by **, *panel 6*) is UDP and was confirmed by ¹H NMR (data not shown). *B*, purified recombinant RsU4kpxs (10 μ g) was mixed with UDP-GlcA, buffer, and NAD⁺ at 37 °C for 15 min (*panel 2*), 45 min (*panel 3*), or 90 min (*panel 4*). The reaction products were separated on a C18 column (Agilent prep-C18), and chromatograms are shown. UDP-4-keto-pentose is marked by an asterisk (*panels 2–4*), and the peak for UDP-xylose is marked by an arrow (*panels 3* and *4*).

(10 μ g) was further incubated with UDP-4-keto-pentose isolated from C18 column (Fig. 10). The conversion to UDP-xylose is clearly enzymatic (Fig. 10, *panel 4*) and requires exogenous NADH (Fig. 10, *panel 4*). NADH is required for the enzymatic reduction step of UDP-4-keto-pentose, resulting in the formation and release of NAD⁺ and UDP-xylose (Fig. 1B). The analog of NADH, NADPH, cannot substitute for NADH (data not shown). Kinetics analyses of UDP-xylose synthase activity of RsU4kpxs are summarized in Table 1, with K_m values of 152.9 μ M (UDP-4-keto-pentose) and 94.2 μ M (NADH); with V_{max} values (μ M min⁻¹) of 3.6 (UDP-4-keto-pentose) and 3.9 (NADH) and with k_{cat}/K_m values (s⁻¹ mM⁻¹) of 0.081 (UDP-4-keto-pentose) and 0.145 (NADH). The relatively lower activity of converting UDP-4-keto-pentose to UDP-xylose cannot be explained by the affinity to the cofactor because the K_m values for NAD⁺ and NADH are similar (113 and 94 μ M, respectively). However, the 150-fold difference in catalytic efficiency (k_{cat}/K_m) between the two activities of the enzyme toward UDP-GlcA (12.8) and UDP-4-keto-pentose (0.081) reflects the partly

different affinity for the respective UDP-sugar but more significantly the actual rate of catalysis (Table 1).

NMR Analysis of the Enzymatic Product, UDP-Xyl—As described in the previous section for the UDP-4-keto-pentose, specific deuteration was observed at C5 in the xylose ring when the reaction was carried out in 90% D₂O. Isolating and purifying the deuterated UDP-xylose product and subsequent analysis via 900-MHz NMR spectrometer (supplemental Fig. S2 and Table S1) allowed a definitive assignment of the pro-R H5 (equatorial) and pro-S H5 (axial) protons. Although the signals from the geminal H5 protons are almost fully overlapped and typically are reported at a single chemical shift (18, 31), at high fields they can be resolved enough to be identified. Fig. 11 (*panel 1*) shows the region of the proton spectrum of UDP-xylose containing the pro-R equatorial H5 (H5e, δ 3.713, $J_{5e,4} = 6.5$ Hz, $J_{5e,5a} = 11.3$ Hz), the pro-S axial H5 (H5a, δ 3.699, $J_{5a,4} = 9.5$ Hz, $J_{5a,5e} = 11.3$ Hz) and H3 (δ 3.661, $J_{3,4} = J_{3,2} = 9.5$). Fig. 11 (*panel 2*) shows the spectrum of the mixture of protonated and deuterated enzymatic products, with additional signal for pro-S axial proton (δ 3.681, $J_{5a,4} = 9.5$ Hz, $J_{5a,D} < 2$ Hz, marked by an asterisk) caused by the deuterated form of the C5 pro-R position. A simulation of the spectrum (Spinevolution program) (32) is shown in Fig. 11 (*panel 3*). It is clear that the additional doublet of H5 geminal to the deuterated D5 (Fig. 11, *panel 3*, H5a(d)) has a large scalar coupling (9.5 Hz) to H4, which is consistent with its axial configuration, and is isotopically shifted upfield by a similar amount observed in the deuterated UDP-4-keto-pentose.

DISCUSSION

We have described the cloning and biochemical characterization of a bi-functional UDP-4-keto-pentose/UDP-xylose synthase from the bacterial plant pathogen *R. solanacearum* str. GM11000. The lower catalytic efficiency of the enzyme to form UDP-xylose from UDP-4-keto-pentose is consistent with the lower level of xylosyl residues found on Ralstonia LPS, when compared with the 4-amino-4-deoxy-L-arabinose (L-Ara4N) residues (33).

Recent carbohydrate analyses of the *R. solanacearum* LPS (composed of lipid A, a core oligosaccharide and an O-polysaccharide) reveal the occurrence of L-Ara4N linked to a heptose

UDP-4-keto-pentose/UDP-xylose Synthase in *R. solanacearum*

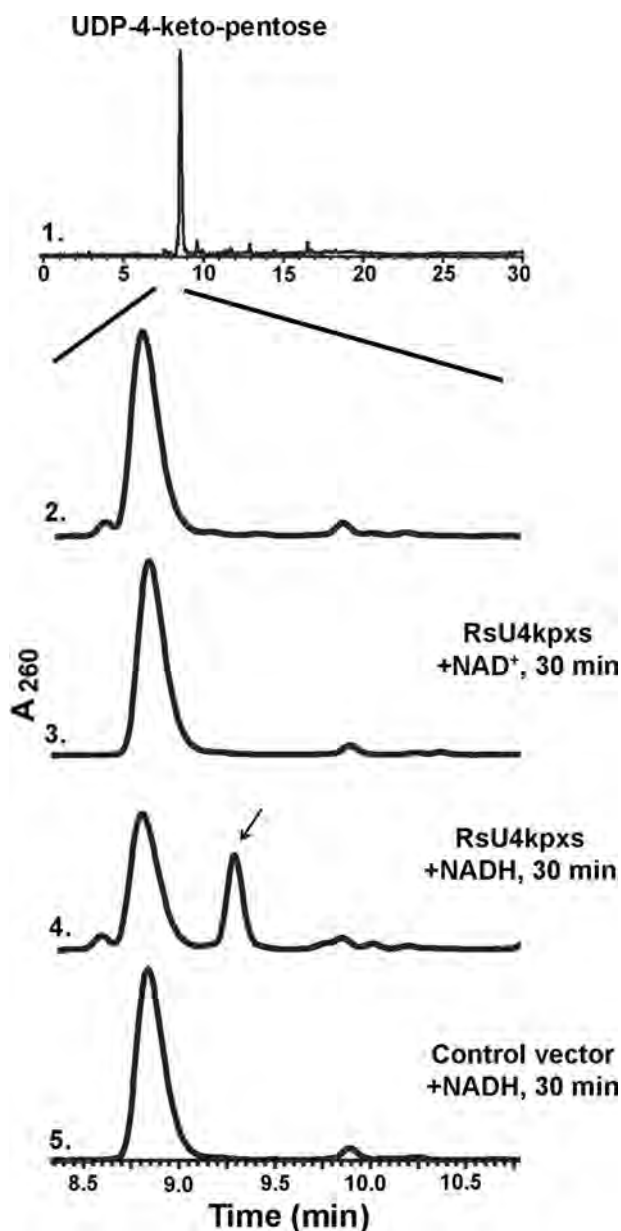


FIGURE 10. The conversion of UDP-4-keto-pentose to UDP-xylose by RsU4kpxs requires exogenous NADH. UDP-4-keto-pentose was enzymatically produced (*panel 1*) under normal assay condition; column-purified (see expanded view in *panel 2*) and used in the following assays. Purified recombinant RsU4kpxs (10 μ g) was incubated with 0.4 mM UDP-4-keto-pentose in the presence of 0.5 mM NAD⁺ (*panel 3*) or 0.5 mM NADH (*panel 4*) at 37 °C for 30 min. As a control, the corresponding column-purified protein isolated from cells expressing empty vector was incubated with UDP-4-keto-pentose and NADH for 30 min (*panel 5*). Reaction products were separated on C18 column (Agilent prep-C18 scalar), and chromatograms are shown. The enzymatic product (*panel 4*) was marked by an arrow, eluted at the same retention time as authentic UDP-xylose, collected, and analyzed by ¹H NMR. The identity of the peak marked by an arrow is UDP-xylose as determined by NMR (data not shown).

residue of the core oligosaccharide (33), as well as a trace amount of a xylosyl residue linked to a rhamnose of the *O*-polysaccharide (33–35) (*supplemental Fig. S3A*). Therefore, the presence of an enzyme activity of RsU4kpxs that produces UDP-xylose precursors in *R. solanacearum* is consistent with the presence of xylose modified LPS in that organism. Because no UDP-GlcA decarboxylase (Uxs) homologs were found in the

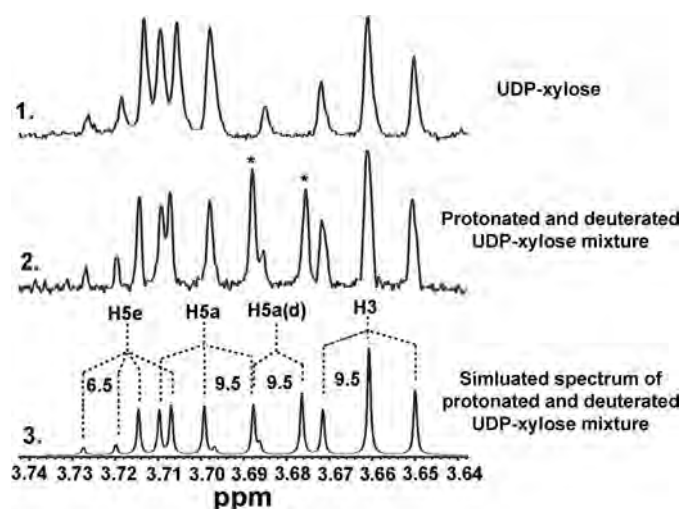


FIGURE 11. 900-MHz proton NMR spectra of the selectively deuterated UDP-xylose. Shown are regions of the proton spectra of UDP-xylose showing selective deuteration at the equatorial (pro-*R*) H5 position. *Panel 1* shows a spectrum (from 3.64 to 3.74 ppm) of UDP-xylose that is fully protonated (C5-H_e/H₃). *Panel 2* shows a spectrum of UDP-xylose (C5-H_e/H₃ and C5-D_e/H₃ mixture) isolated from the enzyme reaction in 90% D₂O. *Panel 3* shows a simulated spectrum of the mixture of fully protonated and selectively deuterated UDP-xylose; H5e and H5a are the equatorial and axial protons at C5, respectively; H5a(d) is the axial proton where the equatorial position is deuterated; the doublet caused by the deuterated form is marked with an asterisk. All of the above spectra were collected via 900-MHz ¹H NMR at 25 °C.

genome of *R. solanacearum*, it is likely that RsU4kpxs is the only protein that provides UDP-xylose in this organism along with UDP-4-keto-pentose.

The operon comprising RsU4kpxs in *Ralstonia* is similar yet distinct from a similar operon in *E. coli* and *Salmonella enterica* (*supplemental Fig. S3B*). In the latter, a gene cluster encoding several proteins (*supplemental Fig. S3*) involved in producing undecaprenyl-4-deoxy-4-formamido-*L*-arabinose, a key intermediate in the biosynthesis of *L*-Ara4N-modified LPS, has been discovered (36, 37). Some of these gene products have been biochemically characterized (19, 38, 39). In *E. coli*, one single polypeptide named ArnA is comprised of two domains: N-terminal formyl-transferase domain and C-terminal decarboxylase domain. This polypeptide has the ability to interconvert UDP-GlcA to UDP-4-keto-pentose (also named UDP-*L*-Ara4O; *supplemental Fig. S3C, panel 1*) and, subsequently after ArnB function, converts the product to UDP- β -4-deoxy-4-formamido-*L*-arabinose (19, 39). In *R. solanacearum*, however, the “equivalent *E. coli* ArnA gene” is split to two separate gene products: the RsU4kpxs characterized in this report and a second gene likely encodes the formyl-transferase (*supplemental Fig. S3B*). We thus proposed that the *Ralstonia RsU4kpxs* gene was likely diverged from the ArnA and further acquired dual enzymatic roles: The first is to produce UDP-4-keto-pentose as precursor for the biosynthesis of *L*-Ara4N modified core oligosaccharide. The second role is to form UDP-xylose where it can serve as precursor for synthesis of xylose containing *O*-polysaccharide (*supplemental Fig. S3C, panel 2*). To determine the *in vivo* function of RsU4kpxs, we have tried to disrupt the expression of the gene. However, numerous attempts to knock out *RsU4kpxs* gene in *R. solanacearum* turned out to be unsuccessful, suggesting that this gene is critical for this organism.

UDP-4-keto-pentose/UDP-xylose Synthase in *R. solanacearum*

A fundamental question regarding the evolution of eukaryotic Uxs and Uaxs enzymes is when their functions diverged from each other (see two possible models in supplemental Fig. S4). Based on blast comparisons and phylogenetic analysis, the UXS clade includes eukaryote (animal, fungus, and plant) Uxs and bacterial Uxs homologs (clade A), whereas the UAXS clade has only plant members. The plant UAXS is more closely related to the bacterial ArnA and RsU4kpxs, than it is to the plant UXS as shown in Fig. 2A. These results imply that plant UAXS did not evolve from a plant UXS, although they both use the same substrates and formed the same intermediates. Several eubacteria, including cyanobacteria, have UXS homologs with more sequence identity to the plant UXS (E-value $1e-129$) than to the plant UAXS, bacterial ArnA homologs, and Clade B U4kpxs proteins. These analyses suggest that an ancestral UXS/UAXS arose in early prokaryotes (see model 1) and then separated into two enzymes (early bacterial UXS and UAXS) with distinct functions. The early bacterial UXS gave rise to the current UXS homologs found in bacteria, animals, fungi, and plants; the early bacterial UAXS then gave rise to the current plant Uaxs, bacterial ArnA homologs, and clade B proteins. During evolution, the plant UAXS further acquired a different function than RsU4kpxs, generating both UDP-apirose and UDP-xylose via the same UDP-4-keto-pentose intermediate. When the early plants acquired both the UAXS and UXS gene from ancestral bacteria remains uncertain.

Acknowledgments—We thank Dr. Russell Malmberg and Malcolm O'Neil for constructive comments on the manuscript.

REFERENCES

- Götting, C., Kuhn, J., Zahn, R., Brinkmann, T., and Kleesiek, K. (2000) *J. Mol. Biol.* **304**, 517–528
- Kuhn, J., Götting, C., Schnölzer, M., Kempf, T., Brinkmann, T., and Kleesiek, K. (2001) *J. Biol. Chem.* **276**, 4940–4947
- Bakker, H., Oka, T., Ashikov, A., Yadav, A., Berger, M., Rana, N. A., Bai, X., Jigami, Y., Haltiwanger, R. S., Esko, J. D., and Gerardy-Schahn, R. (2009) *J. Biol. Chem.* **284**, 2576–2583
- Cherniak, R., and Sundstrom, J. B. (1994) *Infect. Immun.* **62**, 1507–1512
- Vaishnav, V. V., Bacon, B. E., O'Neill, M., and Cherniak, R. (1998) *Carbohydr. Res.* **306**, 315–330
- Klutts, J. S., and Doering, T. L. (2008) *J. Biol. Chem.* **283**, 14327–14334
- O'Neill, M., and York, W. S. (2003) in *The Plant Cell Wall: Annual Plant Review* (Rose, J. K. C., ed) pp. 1–54, Blackwell Publishing and CRC Press, Oxford
- Mohnen, D. (2008) *Curr. Opin. Plant Biol.* **11**, 266–277
- Shashkov, A. S., Arbatsky, N. P., Cedzynski, M., Kaca, W., and Knirel, Y. A. (1999) *Carbohydr. Res.* **319**, 199–203
- Knirel, Y. A., Paramonov, N. A., Vinogradov, E. V., Shashkov, A. S., Dmitriev, B. A., Kochetkov, N. K., Kholodkova, E. V., and Stanislavsky, E. S. (1987) *Eur. J. Biochem.* **167**, 549–561
- Ma, L., Lu, H., Sprinkle, A., Parsek, M. R., and Wozniak, D. J. (2007) *J. Bacteriol.* **189**, 8353–8356
- Xu, X., Ruan, D., Jin, Y., Shashkov, A. S., Senchenkova, S. N., Kilcoyne, M., Savage, A. V., and Zhang, L. (2004) *Carbohydr. Res.* **339**, 1631–1636
- Forsberg, L. S., and Carlson, R. W. (2008) *J. Biol. Chem.* **283**, 16037–16050
- Hwang, H. Y., and Horvitz, H. R. (2002) *Proc. Natl. Acad. Sci. U.S.A.* **99**, 14218–14223
- Mølhøj, M., Verma, R., and Reiter, W. D. (2003) *Plant J.* **35**, 693–703
- Guyett, P., Glushka, J., Gu, X., and Bar-Peled, M. (2009) *Carbohydr. Res.* **344**, 1072–1078
- Gu, X., Wages, C. J., Davis, K. E., Guyett, P. J., and Bar-Peled, M. (2009) *J. Biochem.* **146**, 527–534
- Harper, A. D., and Bar-Peled, M. (2002) *Plant Physiol.* **130**, 2188–2198
- Breazeale, S. D., Ribeiro, A. A., and Raetz, C. R. (2002) *J. Biol. Chem.* **277**, 2886–2896
- Altschul, S. F., Madden, T. L., Schäffer, A. A., Zhang, J., Zhang, Z., Miller, W., and Lipman, D. J. (1997) *Nucleic Acids Res.* **25**, 3389–3402
- Katoh, K., Kuma, K., Toh, H., and Miyata, T. (2005) *Nucleic Acids Res.* **33**, 511–518
- Guindon, S., and Gascuel, O. (2003) *Syst. Biol.* **52**, 696–704
- Gu, X., and Bar-Peled, M. (2004) *Plant Physiol.* **136**, 4256–4264
- Mohnen, D., Bar-Peled, M., and Somerville, C. R. (2008) in *Biosynthesis of Plant Cell Walls* (Himmel, M., ed) pp. 1–54, Blackwell Publishing, Oxford
- Rao, S. T., and Rossmann, M. G. (1973) *J. Mol. Biol.* **76**, 241–256
- Weirenga, R. K., Terpstra, P., and Hol, W. G. (1986) *J. Mol. Biol.* **187**, 101–107
- Tello, M., Rejzek, M., Wilkinson, B., Lawson, D. M., and Field, R. A. (2008) *Chembiochem.* **9**, 1295–1302
- Melançon, C. E., 3rd, Hong, L., White, J. A., Liu, Y. N., and Liu, H. W. (2007) *Biochemistry* **46**, 577–590
- Williams, G. J., Breazeale, S. D., Raetz, C. R., and Naismith, J. H. (2005) *J. Biol. Chem.* **280**, 23000–23008
- Gatzeva-Topalova, P. Z., May, A. P., and Sousa, M. C. (2004) *Biochemistry* **43**, 13370–13379
- Pauly, M., Porchia, A., Olsen, C. E., Nunan, K. J., and Scheller, H. V. (2000) *Anal. Biochem.* **278**, 69–73
- Veshtort, M., and Griffin, R. G. (2006) *J. Magn. Reson.* **178**, 248–282
- Zdorovenko, E. L., Vinogradov, E., Wydra, K., Lindner, B., and Knirel, Y. A. (2008) *Biomacromolecules* **9**, 2215–2220
- Kocharova, N. A., Knirel, Y. A., Shashkov, A. S., Nifant'ev, N. E., Kochetkov, N. K., Varbanets, L. D., Moskalenko, N. V., Brovarskaya, O. S., Muras, V. A., and Young, J. M. (1993) *Carbohydr. Res.* **250**, 275–287
- Varbanets, L. D., Vasil'ev, V. N., and Brovarskaia, O. S. (2003) *Mikrobiologiya* **72**, 19–25
- Gunn, J. S., Lim, K. B., Krueger, J., Kim, K., Guo, L., Hackett, M., and Miller, S. I. (1998) *Mol. Microbiol.* **27**, 1171–1182
- Raetz, C. R., and Whitfield, C. (2002) *Annu. Rev. Biochem.* **71**, 635–700
- Breazeale, S. D., Ribeiro, A. A., and Raetz, C. R. (2003) *J. Biol. Chem.* **278**, 24731–24739
- Breazeale, S. D., Ribeiro, A. A., McClerren, A. L., and Raetz, C. R. (2005) *J. Biol. Chem.* **280**, 14154–14167